Polymer 339 (2025) 129189

Contents lists available at ScienceDirect

Polymer

journal homepage: www.elsevier.com/locate/polymer

UV-crosslinked biomaterials: Functionalized polyethylene glycol for tissue adhesive applications

T. Cernadas [a,b,c], M. Ferreira [a], B.L. Melo [c,d], D. de Melo-Diogo [d], I.J. Correia [a,c,d], P. Ferreira [a,b,e,**], P. Alves [a,f,*]

[a] University of Coimbra, CERES, Department of Chemical Engineering, 3030-790, Coimbra, Portugal
[b] Research Centre for Natural Resources, Environment and Society (CERNAS), Polytechnic Institute of Coimbra, Coimbra, 3045-601, Portugal
[c] AEROG-LAETA, Aerospace Sciences Department, Universidade da Beira Interior, Covilhã, Portugal
[d] RISE-Health, Departamento de Ciências Médicas, Faculdade de Ciências da Saúde, Universidade da Beira Interior, Av. Infante D. Henrique, 6200-506, Covilhã, Portugal
[e] Polytechnic University of Coimbra, Applied Research Institute, Rua da Misericórdia, Lagar dos Cortiços – S. Martinho do Bispo, 3045-093, Coimbra, Portugal
[f] University of Coimbra, CEMMPRE, ARISE, Department of Mechanical Engineering, Rua Luís Reis Santos, 3030-788, Coimbra, Portugal

ARTICLE INFO

Keywords:
Tissue adhesive
Polyethylene glycol
Functionalization
Photocrosslinking
Cytocompatibility

ABSTRACT

Surgeons around the world face the challenge of effectively and securely treat acute wounds. The most used techniques used to reestablish proper tissue continuity and promote healing comprise surgical tape strips and wound suturing or stapling. However, these have different limitations associated, like additional tissue trauma and patient discomfort. Tissue adhesives have emerged as a promising alternative to traditional wound dressings and have been widely explored for their potential to minimize these drawbacks while improving overall outcomes.

This study focused on the preparation of photocrosslinkable biomaterials, synthesized from polyethylene glycol (PEG) functionalized with 2-isocyanatoethyl acrylate (AOI), for potential use as tissue adhesives. The synthesized polymers were then crosslinked using two different UV irradiation times (30 and 120 s) to assess how the crosslinking period impacts the final properties of the films. The materials' chemical composition and thermal and mechanical behavior were further characterized. Rheologic profile, gel content, hydrolytic degradation, and contact angles were assessed. In addition, cytocompatibility evaluation was also conducted. Overall, the obtained data suggest that the newly synthesized tissue adhesives form flexible, homogeneous, and transparent matrices, exhibiting promising properties for potential tissue adhesive applications.

1. Introduction

In recent years, tissue adhesives have made considerable progress, driven by the growing demand for safer and less invasive ways to accomplish the wound healing. Unlike other widely used mechanical techniques, tissue adhesives hold wound edges by covering the entire wound area with a temporary protection barrier, more effectively sealing wounds [1,2]. Therefore, a suitable tissue adhesive must combine an adequate viscosity prior to *in situ* application, a fast-curing rate at physiological temperature, biocompatibility, biodegradability, and good mechanical performance throughout the treatment [3,4]. Oppositely, conventional methods such as sutures and staples, although efficient, frequently cause tissue trauma and inflammation and often require subsequent removal, leading to patient discomfort and even other complications [5,6].

Photocrosslinkable tissue adhesives are a promising alternative since they reduce tissue damage, promote better healing, and are easy to apply [7]. This technique uses UV irradiation to initiate a reaction within specific polymers, transforming them from liquid to solid, and creating a three-dimensional structure with a strong adhesive bond. This approach takes advantage of specifically designed monomers and polymers that, along with a photoinitiator and UV light, allows a control over the material's setting time and mechanical properties at lower costs [8,9].

Several studies [10–12] have focused on developing

* Corresponding author. University of Coimbra, CERES, Department of Chemical Engineering, 3030-790, Coimbra, Portugal.
** Corresponding author. University of Coimbra, CERES, Department of Chemical Engineering, 3030-790, Coimbra, Portugal.
E-mail addresses: paula.ferreira@ipc.pt (P. Ferreira), patricia.alves@dem.uc.pt (P. Alves).

https://doi.org/10.1016/j.polymer.2025.129189
Received 18 July 2025; Received in revised form 16 September 2025; Accepted 5 October 2025
Available online 9 October 2025

photocrosslinkable polymers for use as tissue adhesives. However, these approaches typically require solvent-based processing or multi-step synthesis. In contrast, the present study introduces a streamlined, solvent-free method for producing UV-crosslinkable bioadhesives using PEG and 2-isocyanatoethyl acrylate (AOI), a promising monomer in this context. AOI has previously demonstrated favorable reactivity and mechanical performance, yielding promising results [10,13,14]. However, its use in bioadhesive systems remains underexplored.

PEG is a hydrophilic, non-ionic polymer widely recognized for its biocompatibility, making it an ideal candidate for various medical applications [15,16]. In particular, PEG's ability to be easily modified and its flexibility in forming hydrogels further enhance its utility in developing tissue adhesives [8]. However, PEG is inert and cannot create a stable network; therefore, a suitable functional group, such as acrylate, must be introduced to enable crosslinking [17]. Thus, the functionalization of PEG with AOI introduces acrylate groups into the polymer chain, which are known for their efficient photocrosslinking capabilities under UV irradiation. So, while acrylates can rapidly crosslink under UV irradiation, isocyanates exhibit high reactivity with amines in living tissues [4,18].

The synthesis of these photocrosslinkable biomaterials through the reaction of PEG 600 with AOI represents a novel and streamlined strategy in the field of surgical materials. Additionally, the use of UV light for crosslinking grants on-demand activation, allowing surgeons to precisely control the setting process during surgical procedures [19]. This work contributes not only by proposing a practical and scalable formulation route but also by providing a comprehensive physicochemical and thermal characterization to assess crosslinking efficiency, stability, and mechanical behavior under physiologically relevant conditions to enhance patient outcomes, reduce surgical times, and minimize postoperative complications. Altogether, this research aims to explore the synthesis, characterization, and potential applications of these novel photocrosslinkable adhesives, thereby contributing to the advancement of medical adhesive technologies and enhancing surgical practices.

2. Experimental procedures

2.1. Materials

Polyethylene glycol (PEG 600, Mn ≈ 600) was acquired from Clariant (Muttenz, Switzerland). 2-isocyanatoethyl acrylate (AOI, 99 %) was purchased from BLDPharm (Shanghai, China). Hydroquinone, formamide (99 %), diiodomethane (99 %), phosphate-buffered saline tablets (PBS), Dulbecco's modified Eagle's medium F-12 (DMEM-F12), penicillin/streptomycin, trypsin and resazurin were purchased from Sigma-Aldrich (Sintra, Portugal). Diethyl ether (99 %), toluene (100 %), and anhydrous calcium chloride (96 %) were bought from ACROS organics (Geel, Belgium).

Photoinitiator 2-hydroxy-1-[4-(2-hydroxyethoxy) phenyl]-2-methyl-1-propanone, trade name Irgacure® 2959 (Ir2959), was kindly provided by BASF (Germany). The deuterated chloroform ($CDCl_3$) used as solvent was purchased from Eurisotop (Saint-Aubin, France). All reagents, except PEG 600, were used as received without further purification.

Normal human dermal fibroblasts (NHDF) cells were purchased from Promo-Cell (Heidelberg, Germany). Fetal bovine serum (FBS) was obtained from Biochrom AG (Berlin, Germany).

2.2. Methods

2.2.1. Water removal from PEG 600

Azeotropic distillation with toluene was used to remove water from PEG (25 % (w/v)). The two components were added to a round-bottom flask connected to a Barrett distilling receiver. This receiver was connected to a condenser, with a drying tube applied to the top. Distillation was carried out for approximately 2 h at 170 °C. The procedure temperature was controlled with a silicone bath on a heating mantle equipped with a magnetic stir bar. Once the desired amount of distillate had been collected, it was allowed to cool to room temperature so it could be properly sealed and stored for later use.

2.2.2. Functionalization of anhydrous PEG 600 with AOI

The hydroxyl groups of anhydrous PEG were modified with the isocyanate groups in AOI, leading to the formation of urethane bonds. PEG functionalization with AOI was carried out using a 2:1 AOI:PEG ratio in a three-neck round-bottom flask equipped with a nitrogen inlet, a water glass collector, and a water condenser. A drying tower filled with calcium chloride was placed atop the condenser to prevent moisture from entering the reaction system. The mixture was heated in an oil bath at 55 °C and continuously stirred magnetically. Hydroquinone (0.02 % of the total monomer weight) was added as an inhibitor to prevent premature crosslinking. AOI was then carefully added dropwise to the solution. After 6 h of reaction, a transparent liquid polymer, PEG-AOI (PA), was obtained. A schematic representation of PEG functionalization with AOI is shown in Scheme 1.

2.2.3. Photocrosslinking and bioadhesives preparation

Photocrosslinking was achieved by adding the photoinitiator (Ir2959) to the previously functionalized polymer in a percentage of 4 % of the carbon double-bond moles (0.3 % w/v). This stoichiometric approach ensures consistent radical generation based on the number of available reactive sites, achieving efficient photopolymerization while maintaining cytocompatibility [20,21].

The reaction flask was protected from light until complete dissolution. The final homogeneous solution was poured onto glass plates and evenly spread using a stainless-steel cylinder. Afterward, it was irradiated using a Multiband UV UVGL-48 lamp from Mineral Light® (wavelengths: 254–354 nm) for either 30 or 120 s. The selected curing times reflect the minimum duration required to obtain handleable films and the maximum exposure considered practical for surgical application.

After UV irradiation, transparent and uniform films with a thickness of 1 mm were obtained. These will be further referred to as PA30 and PA120, respectively. Scheme 2 summarizes the chemical reactions involved in the photocrosslinking process.

2.3. Characterization techniques

2.3.1. Attenuated total reflectance - fourier transform infrared spectroscopy (ATR-FTIR)

The precursor molecules (PEG and AOI), the functionalized PEG (PA), and the photocrosslinked adhesives PA30 and PA120 were characterized by ATR-FTIR analysis using a Frontier FT-NIR/MIR spectrometer from PerkinElmer. Data were collected with a 4 cm^{-1} spectral resolution and 64 scans.

2.3.2. Proton nuclear magnetic resonance (^1H NMR)

^1H NMR spectra of the PEG and AOI monomers and the functionalized PEG (PA) were recorded in a 400 MHz Bruker Advance III Spectrometer (Massachusetts, USA), using a 5 mm broadband NMR probe in deuterated chloroform ($CDCl_3$) at room temperature. Tetramethylsilane (TMS) was used as the internal reference.

2.3.3. Rheological studies

The functionalized PEG (PA) viscosity was studied, at 25 °C and 37 °C, using a controlled stress rheometer, Haake RheoStress, Thermo Fisher Scientific model RS1 (Germany). A plate/plate system (P20–Ti), with titanium for the rotating part and stainless steel for the stationary part was used. Newtonian viscosity was fitted using the Newton (visc) model, obtained using the Haake RheoWin 4.20.005 software (Haake, Germany). The resultant viscosities were determined as a function of the shear rate over time. All measurements were made in triplicate.

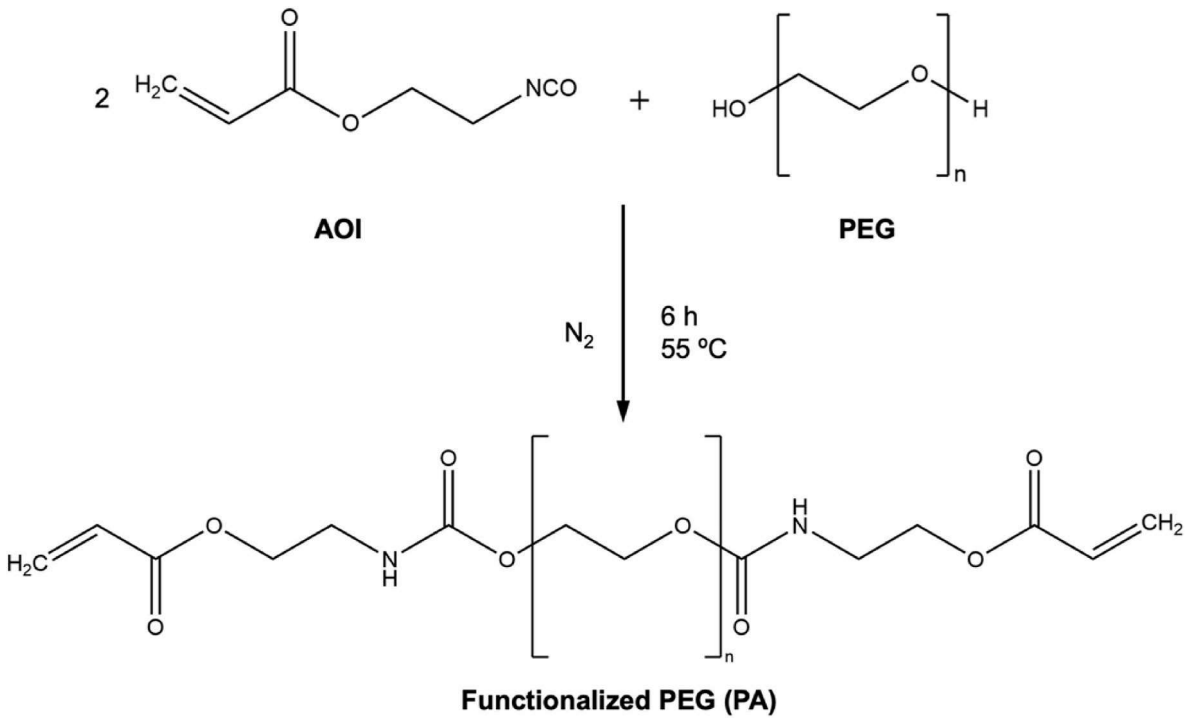

Scheme 1. Schematic representation of PEG functionalization with AOI, leading to the incorporation of photoreactive sites in the final PA structure.

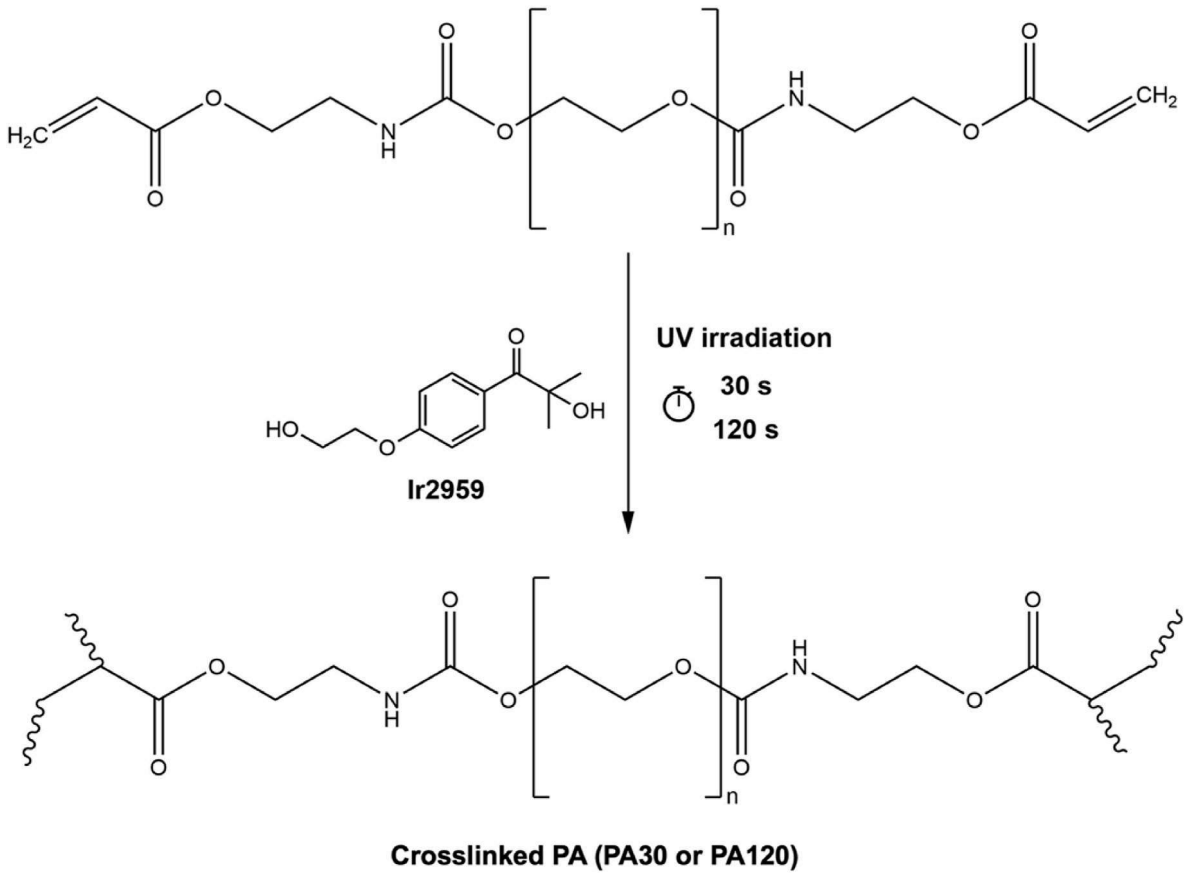

Scheme 2. Schematic representation of photocrosslinking reactions to obtain the crosslinked PA (PA30 and PA120).

2.3.4. Gel content

The gel content of the materials was determined by solvent extraction to provide a qualitative assessment of network formation efficiency. Three samples of each dried film, with the dimensions of 1.25 × 1 × 0.01 cm, were accurately weighted (W_i) and immersed in diethyl ether for 24 h at room temperature under constant stirring, in sealed containers. After extraction, the insoluble (crosslinked) fractions were collected, dried to constant weight, and reweighted (W_f). Gel content was determined as represented in Equation (1), reflecting the proportion of the material that remained insoluble after extraction. This method allows indirect evaluation of the extent of crosslinking through the amount of non-extractable polymer network formed.

$$\text{Gel content}\ (\%) = \left(\frac{W_f}{W_i}\right) \times 100 \quad (1)$$

2.3.5. Thermogravimetric analysis (TGA)

The thermal stability of the photocrosslinked bioadhesive films (PA30 and PA120) was assessed by thermogravimetric analysis (TGA) using a Q500 thermogravimetric analyzer (TA Instruments, USA). Approximately 10 mg of each dried film were placed in a platinum pan and heated from room temperature to 600 °C at a rate of 10 °C/min under a nitrogen atmosphere with a flow rate of 100 mL/min. The resulting thermograms were used to evaluate the degradation profile and estimate the thermal stability of the materials.

2.3.6. Dynamic mechanical thermal analysis (DMTA)

Photocrosslinked polymers (PA30 and PA120) were analyzed by Dynamical Mechanical Thermal Analysis (DMTA) using a Triton Tritec 2000 in the Single Cantilever Bending mode under multifrequency conditions (1 and 10 Hz) with a standard heating rate of 5 °C·min^{-1}. The glass transition temperature (T_g) was determined as the peak in tan δ, calculated by Equation (2).

$$\text{Tan}\ \delta = \frac{E''}{E'} \quad (2)$$

where E″ and E′ are the loss and storage modulus, respectively.

2.3.7. Water sorption capacity

Three samples of each produced film, with the dimensions of 1.25 × 1 × 0.001 cm, were dried under vacuum conditions until constant weight (W_d) and then placed in a desiccator containing a pentahydrate copper sulphate saturated solution, at a relative humidity of 95 % and at room temperature. Specimens of each sample were removed and weighted at predetermined times (24 h, 72 h, 1, 2, 3, 4, 5, and 6 weeks) until maximum weight was achieved (W_s), and the water sorption capacity was assessed using Equation (3).

$$\text{Water sorption}\ (\%) = \left(\frac{W_s\text{-}W_d}{W_d}\right) \times 100 \quad (3)$$

2.3.8. Hydrolytic degradation

Three samples of the developed adhesives, with the dimensions of 1.25 × 1 × 0.001 cm, were previously dried in a vacuum oven at room temperature and then weighted ($W_{d,o}$). Afterward, they were immersed in PBS (0.01 M, pH 7.4) and then incubated for six weeks at 37 °C. At distinct established times (24 h, 72 h, 1, 2, 3, 4, and 6 weeks), the films were removed from PBS, washed with distilled water, and dried in vacuum conditions at 37 °C until constant weight ($W_{d,t}$). The degree of degradation was calculated from weight loss, as presented in Equation (4).

$$\text{Weight loss}\ (\%) = \frac{W_{d,0}\text{-}W_{d,t}}{W_{d,0}} \times 100 \quad (4)$$

where $W_{d,o}$ and $W_{d,t}$ are the samples average weights before the degradation test and at time *t*, respectively.

2.3.9. Dynamic water contact angles

Dynamic water contact angles of PA30 and PA120 materials were measured using a Dataphysics OCA-20 contact angle analyzer (DataPhysics Instruments, Filderstadt, Germany) with the sessile drop method. A 10 μL droplet of deionized water was automatically dispensed onto the sample surface, and its evolution over 120 s was recorded with a CCD video camera. Water contact angles were calculated automatically by the instrument's software. The reported data represent the mean values from at least three independent drop deposition measurements.

2.3.10. Surface energy by contact angle measurement

The surface energies of the photocrosslinked adhesives (PA30 and PA120) were evaluated by static contact angle (θ) measurements with a Dataphysics OCA 20 analyzer. The results were then compared with the values reported in the literature for skin and blood tissues. All the tests were performed on the air-facing surfaces of the samples with four liquids: water, ethylene glycol, formamide, and diiodomethane, using the sessile drop method. Ten measurements on different points were performed to calculate the mean static contact angle θ and its standard deviation. The surface free energies (γ_S) of each film and of the gelatine sheet, along with their dispersive (γ_S^D) and polar (γ_S^P) components, were determined according to the Owens-Wendt-Rabel and Kaelble (OWRK) method.

2.3.11. Cytocompatibility evaluation

The cytocompatibility of the PA30 and PA120 materials was evaluated using NHDF through the resazurin assay, as previously described by Pontinha et al. with slight modifications [22]. The NHDF were cultured in 75 cm^2 t-flasks, using DMEM-F12 medium supplemented with FBS (10 % (v/v)) and penicillin/streptomycin (1 % (v/v)) in an incubator containing a humidified atmosphere (37 °C, 5 % CO_2).

To determine the cytocompatibility of the PA30 and PA120 materials, the NHDF were initially seeded in 24-well plates at a cell density adjusted to their total incubation time with the materials (*i.e.*, 1, 3, and 7 days) to avoid any chance of cell death due to NHDF confluence. In this way, NHDF were seeded at a density of 30 × 10^3, 15 × 10^3, and 3 × 10^3 cells/well for the incubation times of 1, 3, and 7 days, respectively, with the PA30 and PA120 materials. After 48 h of seeding the NHDF, these were incubated with the PA30 and PA120 materials (with sizes below 10 % of the well area in fresh culture medium; according to ISO 10993–5/12) for 1, 3, and 7 days. At the end of each time point, the materials were removed, and the NHDF were incubated with resazurin (10 % (v/v) in fresh culture medium) for 4 h in the dark (37 °C, 5 % CO_2). Then, the fluorescence of resorufin was analyzed in a Spectramax Gemini EM spectrofluorometer (λ_{ex} = 560 nm; λ_{em} = 590 nm) to determine the NHDF viability. NHDF only incubated with culture medium (*i.e.*, without the materials) were used as the negative control (K^-). Medium with just resazurin (*i.e.*, without cells and without any materials) was used as the background. The Cell viability (%) was calculated as presented in Equation (5) [23].

$$\text{Cell viability}\ (\%) = \frac{Fluorescence_{treated} - Fluorescence_{background}}{Fluorescence_{negative\ controls} - Fluorescence_{background}} \times 100 \quad (5)$$

The growth/morphology of NHDF after each incubation period with the materials (*i.e.*, prior to the resazurin incubation step) was visualized in an Olympus CX41 inverted light microscope (Tokyo, Japan) equipped with an Olympus SP-500 UZ digital camera.

2.3.12. Statistical analysis

The one-way analysis of variance with the Student–Newman–Keuls test was used by authors for multiple group comparisons. The trial version of GraphPad Prism v6.0 (Software, CA, USA) was used for data analysis. A *p*-value lower than 0.05 ($p < 0.05$) was considered statistically significant.

3. Results and discussion

3.1. Synthesis

The previously described experimental procedures allowed for preparing PEG-based films, which underwent comprehensive characterization, including chemical, thermal, mechanical, and cytocompatibility assessments.

The preparation of these films involved three key steps: i) azeotropic distillation of PEG 600, ii) functionalization with AOI to introduce photocrosslinkable carbon-carbon double bonds, and iii) UV crosslinking.

Since isocyanate groups (NCO) are highly reactive with water, removing moisture from PEG is essential to prevent interference with the desired reaction and to maintain the quality and properties of the final polyurethane acrylate product. Azeotropic distillation was performed to ensure PEG dryness for more efficient and controlled functionalization with AOI. Additionally, this method minimizes unwanted side reactions, such as the reaction between isocyanates and water, which can lead to foaming due to carbon dioxide release [24]. After azeotropic distillation, PEG was modified with AOI, a bifunctional monomer containing both an isocyanate (NCO) and an acrylate (-C═CH_2) group. This structure enables AOI to react with PEG hydroxyl groups, forming urethane linkages. Moreover, its acrylate group facilitates the photocrosslinking of the functionalized PEG (referred to as PA). At the end of the reaction, PA exhibited a viscous, colorless, oily appearance, indicating its potential for *in situ* injection applications.

Finally, the cytocompatible photoinitiator Irgacure® 2959, widely used in the biomedical field, was mixed into PA to achieve instantaneous crosslinking under mild conditions. After 30 or 120 s of UV irradiation, flexible and transparent films (PA30 and PA120, respectively) were formed and subsequently characterized to assess their properties.

3.2. Chemical characterization

ATR-FTIR spectroscopy and ^{1}H NMR allowed a follow-up of the functionalization and photocrosslinking reactions by identifying the functional groups of the monomers and reaction products. The ATR-FTIR spectra of the precursor molecules (PEG and AOI), the functionalized PEG (PA), and the photocrosslinked adhesives PA30 and PA120 are presented in Fig. 1.

Analyzing the AOI spectrum (Fig. 1A), two strong peaks were observed at 2331 cm^{-1} and 1725 cm^{-1}, representing –N═C═O and –C═O stretching, respectively. A smaller peak at 1635 cm^{-1} corresponds to the alkenyl –C═C stretch in AOI. In the PEG spectrum, a band around 3300 cm^{-1} is characteristic of the hydroxyl group (–O-H) stretching vibrations. Additionally, the characteristic stretching vibrations of the –CH_2 bond occurs around 2850 cm^{-1}, and at 1100 cm^{-1}, the –C-O-C stretching vibration of the repeated –OCH_2CH_2- units of the PEG backbone are noted. Finally, in Fig. 1A, the PA spectrum shows the disappearance of the broadband between 3300 and 3600 cm^{-1}, indicating the complete reaction of –OH end-groups alongside the emergence of N–H stretching absorptions at 3340 cm^{-1}, attributed to urethane formation. The formation of the ester group at 1800 cm^{-1}, corresponding to the carbonyl stretch –C═O of AOI, was also observed. The presence of double bonds (–C═C) after functionalization was confirmed by the appearance of a new band at 1680 cm^{-1} and the decreasing intensity of the –N═C═O stretching peak between 2280 and 2350 cm^{-1}. Furthermore, the PA spectrum displays a new signal at 1620 cm^{-1}, attributed to the overlap of signals for –N-H bending and –C-N stretching bands of the urethane bond.

After UV irradiation, the –C═C stretching band in the ATR–FTIR spectra of the networks nearly disappears due to photocrosslinking (Fig. 1B). It is important to emphasize that for potential applications as resorbable tissue adhesives, extensive conversion of free double bonds is essential to minimize the release of potentially reactive and toxic

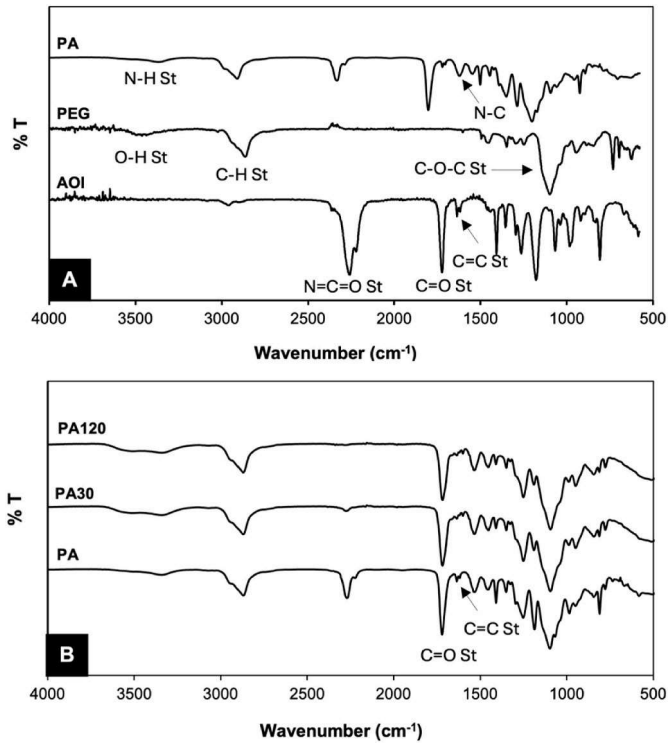

Fig. 1. (A) ATR-FTIR spectra of the precursor molecules (PEG and AOI) and PA before crosslinking, (B) ATR-FTIR spectra of PA and of photocrosslinked PA after 30 (PA30) and 120 s (PA120) of exposure to UV irradiation.

compounds during degradation [25]. Moreover, the UV exposure time required for effective crosslinking was determined based on ATR-FTIR analysis, where the apparent disappearance of peaks associated with the C═C double bond was used as an indicator of conversion efficiency. Results indicated that 30 s of UV exposure (PA30) was sufficient to achieve a high level of C═C bond conversion, leading to stable network formation. In this same spectrum, residual free –N═C═O groups were subtly present. These unreacted isocyanate groups present in the adhesive structure may play a functional role in enhancing adhesion to biological substrates [26].

Like ATR-FTIR, the NMR technique was used to monitor functionalization. The ^{1}H NMR spectra of the initial molecules (PEG and AOI) and the functionalized polymer (PA) are shown in Fig. 2.

The PEG spectrum presented in Fig. 2 corresponds to anhydrous PEG obtained via azeotropic distillation with toluene. Residual toluene impurities were observed at 7.17 ppm and 7.25 ppm (*). The characteristic backbone peaks of PEG are present at 3.59 (g), 3.64 (h), and 3.71 (f) ppm, corresponding to the repeating methylene protons (–CH_2–) of the PEG chain [27]. These are also present in the PA spectrum, showing slight shifts due to changes in the chemical environment during functionalization. This confirms that the PEG backbone remains intact and is not degraded during the reaction and confirms the successful functionalization of PA along with the presence of the signals at approximately 6.46 (d), 6.16 (c), and 5.90 (e) ppm. These signals correspond to the double bonds of AOI's acrylate groups, confirming the unsaturation of the final polymer.

In the AOI spectrum, the methylene proton (-CH_2) directly bonded to the oxygen atom of the isocyanate-ethyl-acrylate (-O-CH_2) is observed at 3.67 ppm (a), while the –CH_2 group adjacent to the carbonyl group (-C═O) appears at 4.20 ppm (b).

Three new signals in the PA spectrum, visible at 4.24 (i), 3.48 (j), and 3.58 (k) ppm, are associated with the methylene groups near the urethane group and the protons of the urethane groups –NH–CH_2- and –NH–C═O, respectively. These new peaks confirm the successful

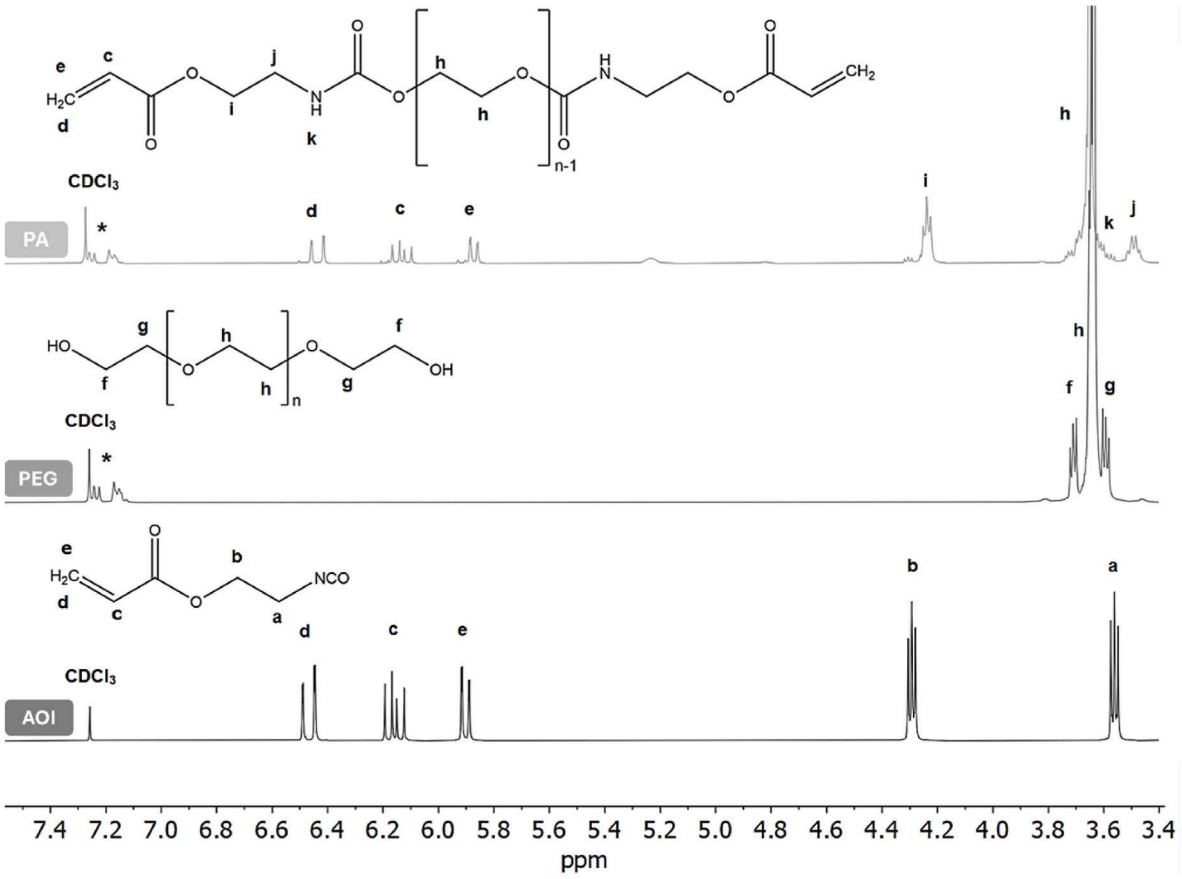

Fig. 2. ^{1}H NMR spectra of AOI, anhydrous PEG, and non-crosslinked PA in deuterated chloroform ($CDCl_3$) at 400 MHz.

formation of urethane bonds, showing that the hydroxyl groups on PEG reacted with the isocyanate group of AOI.

3.3. Rheological studies

Rheological studies were performed with the functionalized PEG (PA) to establish the relationship between viscosity and shear rate (Fig. 3). This analysis was conducted considering the materials storage and application temperatures (25 °C and 37 °C, respectively). Given their intended use as tissue adhesives, the prepared blends must be easy to apply and conform to the injured tissue.

Fig. 3 illustrates the PA's Newtonian behavior, indicating that the viscosities remain constant as the shear rate increases. This property is advantageous for practical applications, as it ensures consistent flow behavior regardless of the applied force or dispensing rate. Additionally, PA exhibited relatively low viscosities, with values ranging from 0.19 to 0.33 Pa s, with the lowest value observed at 37 °C (0.19 Pa s). These values fall within the range reported for commercially available bio-adhesives. For example, fibrin-based glues have been reported to exhibit dynamic viscosities in the range of 0.1–0.2 Pa s [28]. At the same time, PEG-based adhesives used in surgical applications (e.g., FocalSeal by Genzyme Corporation, Cambridge, MA) typically have low viscosities, ranging from 0.7 mPa s to 1.4 Pa s, to ensure they can be easily dispensed through a needle under application conditions [29]. Accordingly, PA's low viscosity (and Newtonian profile) allows it to flow and spread when operated upon gravity or by some other type of force, facilitating its application by various methods. Therefore, the rheological properties of our formulation are consistent with those required for clinical use, further supporting its suitability for tissue adhesive applications.

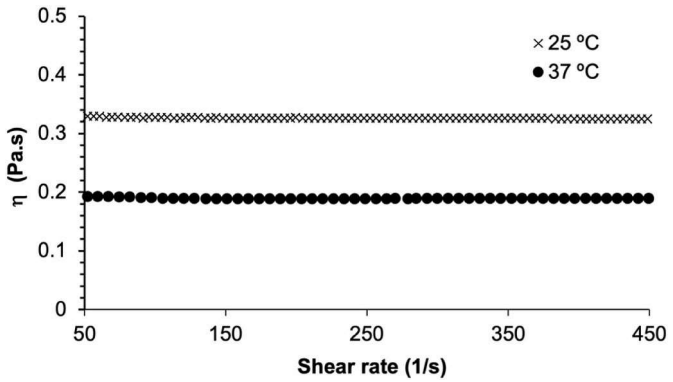

Fig. 3. PA viscosity as a function of shear rate at constant temperature (25 °C and 37 °C).

3.4. Gel content

The extent of network formation was assessed by measuring the materials' gel content, which reflects the amount of unreacted, soluble polymer remaining in the matrix after extraction, and thus serves as a qualitative indicator of crosslinking efficiency.

Table 1 presents the gel content values obtained for two different UV exposure times. The curing times of 30 and 120 s were selected based on

Table 1
UV irradiation times and corresponding gel content of the prepared adhesives.

Adhesive	Photocrosslinking time (s)	Gel content (%)
PA30	30	86.3 ± 1.1
PA120	120	92.0 ± 0.1

preliminary tests and clinical relevance, representing the shortest duration that allowed coherent and handleable film formation and the maximum feasible exposure compatible with surgical procedures. This experimental window was chosen to evaluate how the extent of crosslinking influences material performance under practical conditions.

The results indicate that longer UV exposure leads to a lower soluble fraction, suggesting a higher conversion of C═C bonds and greater network integrity. These findings are consistent with the ATR-FTIR results, which showed residual C═C signals in all samples, confirming that complete curing was not achieved under the tested conditions.

Specifically, gel content increased from 86.3 ± 1.1 % for PA30 to 92.0 ± 0.1 % for PA120, indicating that both formulations underwent substantial network formation, with PA120 achieving a higher degree of insolubilization. While full crosslinking was not accomplished, the 30-s exposure, combined with the selected photoinitiator concentration, was sufficient to achieve a high conversion efficiency.

3.5. Thermal analysis

To further explore the impact of UV exposure on the network stability, Thermogravimetric Analysis (TGA) was performed on both formulations. As shown in Fig. 4, the thermograms of PA30 and PA120 display a similar thermal decomposition profile, with a major degradation event occurring around 410 °C. Notably, a slightly lower weight loss was observed for PA120 in the temperature range below 300 °C, suggesting marginally higher thermal stability.

This behavior is consistent with the gel content data, supporting the statement that PA120 exhibits a denser and more crosslinked polymer network. Despite the subtle differences, the correlation between reduced early-stage mass loss and increased gel fraction reinforces the role of UV exposure time in tuning crosslinking efficiency and thermal stability. Moreover, both formulations demonstrated thermal stability suitable for biomedical applications.

The Dynamic Mechanical Thermal Analysis (DMTA) technique was employed to determine the glass transition temperature (T_g) of the crosslinked materials, providing insight into their thermal and viscoelastic properties. For tissue adhesive applications, the material must remain soft, flexible, and elastomeric at physiological temperature (≈37 °C), ensuring conformability to tissues and adequate mechanical integrity during and after application.

Fig. 5 presents the tan δ curves at a frequency of 1 Hz for both adhesive formulations. The T_g was determined from the temperature corresponding to the maximum of the tan δ peak. The results show that both formulations exhibit T_g values well below physiological temperature, with PA30 at −39 °C and PA120 at −32 °C, and no crystallization was observed. These low T_g values confirm that both materials remain in a rubbery, flexible state under physiological and ambient conditions, a desirable property for soft-tissue applications.

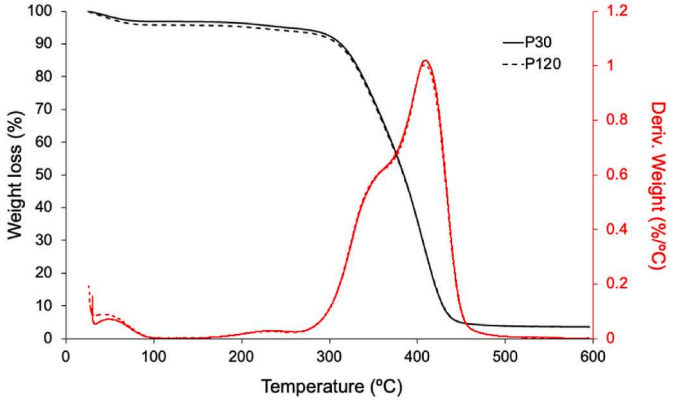

Fig. 4. TGA and derivative thermogravimetric (DTG) curves of PA30 and PA120 bioadhesive films. The TGA curves (black) show the weight loss (%) as a function of temperature, while the DTG curves (red) display the rate of weight loss (%/°C)

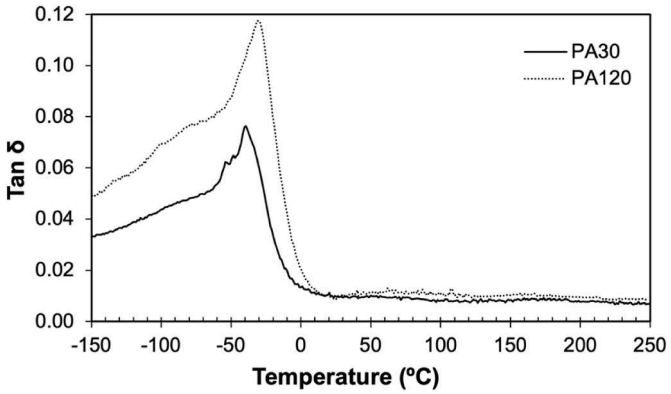

Fig. 5. Traces of tan δ as a function of temperature at 1 Hz for the films prepared by photocrosslinking of PA after 30 (PA30) and 120 (PA120) seconds of UV irradiation.

Moreover, increasing the UV exposure time from 30 to 120 s results in an increase in T_g, indicating reduced chain mobility due to a higher degree of crosslinking. This observation is consistent with the gel contents results, where longer UV exposure led to lower solubilization and improved network formation.

These T_g values are in agreement with previous studies on PEG-based UV-crosslinked systems: for instance, pure crosslinked PEGDA exhibits a T_g of approximately −27 °C in PTMC/PEGDA blends [30], and PEGDMA hydrogels show comparable negative T_g ranges that increase with crosslinking density [31]. Such values are indicative of elastomeric behavior and are suitable for biomedical adhesives designed for application at body temperature.

3.6. Water sorption capacity

After an injury or an incision, the body initiates the wound-healing process to restore the structure and function of damaged tissue as quickly as possible. Tissue adhesives can enhance this process by providing consistent mechanical support, promoting cell interaction and proliferation, and stabilizing the wound area [32]. Additionally, effective wound healing requires the removal of excess exudates, as their accumulation can lead to skin infections and tissue maceration [33]. Tissue adhesives that absorb excess exudates are essential, as they create a moist microenvironment conducive to healing while protecting the wound site [34]. Water sorption, along with the corresponding increase in material volume (swelling), is a crucial factor that can influence the success of the treatment procedure. Fig. 6 illustrates the water sorption percentage of PA30 and PA120 after six weeks of incubation in a water-saturated atmosphere.

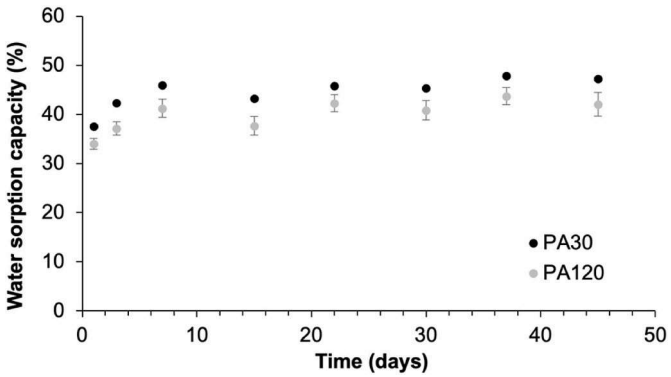

Fig. 6. Water uptake for the synthesized materials at room temperature.

The water sorption results in Fig. 6 indicate that, although the materials display similar swelling behaviors throughout the study period, the water sorption percentage decreases as the irradiation exposure duration increases. Materials subjected to 120 s of UV radiation (PA120) show lower degrees of swelling, with initial values of 34 ± 1.1 % and 42 ± 2.4 % at the end of 45 days. In contrast, PA30 material exhibited swelling values of 37.6 ± 0.3 % on the first day, increasing to 47.3 ± 0.3 % by the end of the study. This difference is likely attributed to the degree of crosslinking, as confirmed by the gel content results, since longer UV-curing times lead to more crosslinked materials with higher retractive (elastic) forces. This results in more stable, compact, and insoluble three-dimensional networks, thereby reducing the available free space within the polymer matrix [35]. The lower swelling percentages of PA120 are consistent with the surface energy results (section 3.8.2), as this material displayed the lowest polar component. Furthermore, no significant changes in water uptake were observed during the 6-week study period, indicating stable swelling behavior of the materials.

The swelling ratio is a valuable indicator of the hydrophilicity and hydrophobicity of the final material. Both materials exhibited relatively high swelling values (approximately 40 %), attributed to the presence of PEG, which is characterized by hydrophilic long chains capable of absorbing significant amounts of water [36]. The threshold at which the swelling pressure of a surgical adhesive becomes harmful to surrounding tissues generally depends on the specific tissue type, adhesive location, and duration of application. PEG-based bioadhesives, such as CoSeal® (which shows over 500 % swelling in 3 days in PBS) and DuraSeal™ (98 % swelling within 24 h), have been effectively applied as tissue sealants in applications like topical wound dressings or as sealants where swelling properties are less critical than in cases involving internal injuries [37]. Zhang et al. identify excessive swelling (50–400 % of the original volume) as a significant limitation of commercial PEG sealants [17]. Therefore, the expected pressure exerted by both PA materials on the wound is lower than that of commercial PEG-based materials and may, therefore, enhance hemostasis [38].

3.7. Hydrolytic degradation

Tissue adhesives can either detach from or be absorbed by the body when no longer needed, making biodegradability a critical feature for biomedical applications, particularly those used in internal wound treatment. To evaluate this property, the hydrolytic degradation of the photocrosslinked materials was assessed. Three samples of each material were immersed in PBS (pH 7.4) and incubated at 37 °C to simulate physiological conditions. The assay was conducted over five weeks, with weight loss monitored over time, as illustrated in Fig. 7.

The results presented in Fig. 7 show that all samples experienced some weight loss within the first day of the experiment (between 17 % and 20 %). This initial weight loss may be attributed to the solubilization of non-crosslinked polymeric chains and low molecular weight compounds, including residual monomers, trapped photoinitiator molecules, and trace amounts of solvent (toluene) [3,13]. Furthermore, the findings reveal that both photocrosslinked PAs maintained hydrolytic stability throughout the study, which is critical for temporary biomedical applications, particularly as wound care materials.

These results align with the fact that while PEG exhibits a highly hydrophilic character, acrylate-based PEG hydrogels lack biodegradability under physiological conditions due to the ether bonds and the carbon–carbon double bonds present in their main chain [39,40]. However, in oxidative environments (such as those at a wound site with immune cell activity), degradation of acrylate crosslinks can be induced, leading to gradual breakdown. In this case, the reaction between PEG and AOI also introduces ester and urethane linkages (–NH–CO-O-), which are more hydrolytically stable than ester linkages but can still degrade slowly in hydrophilic environments [41]. These results demonstrate that the materials maintain their structural and functional integrity, ensuring stability for the necessary duration to hold tissues together until significant tissue regeneration occurs [8].

No major differences were observed between the studied materials regarding the impact of crosslinking time. Still, longer UV exposure times and, consequently, higher crosslinking degrees were associated with lower weight loss values. These findings align with the swelling and gel content analysis and can be attributed to diffusion constraints, as water faces greater resistance when diffusing into a more compact and crosslinked network.

However, it is important to note that these results are based on *in vitro* incubation. Degradation is expected to occur significantly faster in potential *in vivo* applications due to the presence of enzymes, pH levels, oxidative conditions, and cellular components that will influence the degradation process [42]. This evidence allows us to anticipate the capability of tailoring the degradation rates of a material from the initial stages of the production process to fit a specific application (internal or external). This feature is highly advantageous for these new products compared to the currently available non-biodegradable materials.

3.8. Contact angle measurements

One of the most critical surface properties influencing a material's biological performance is its wettability, which determines how it interacts with biological cells and fluids [43]. This property can be evaluated by measuring the dynamic water contact angle (WCA) between a liquid droplet and the material surface. Fig. 8 and Table 2 display the WCA results of PA after 30 s and 120 s of exposure to UV irradiation.

As expected, the results revealed that despite the differences in the initial WCA (32.49° ± 0.34 and 41.33° ± 0.50 for PA30 and PA120, respectively), both materials present comparable profiles and similar final WCA values, confirming their hydrophilic behavior and good wettability. This property enables these materials to maintain a moist

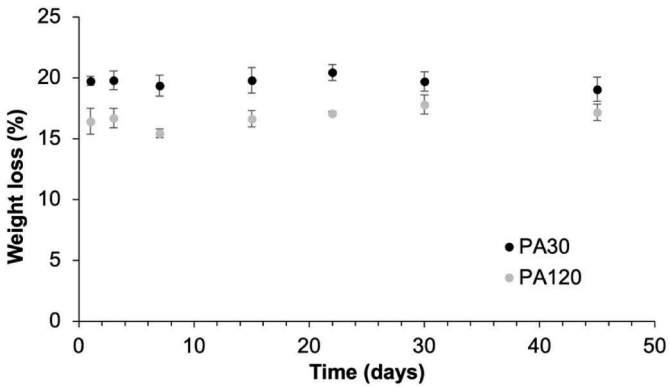

Fig. 7. PA30 and PA120 wt loss during incubation in PBS (pH 7.4) at 37 °C.

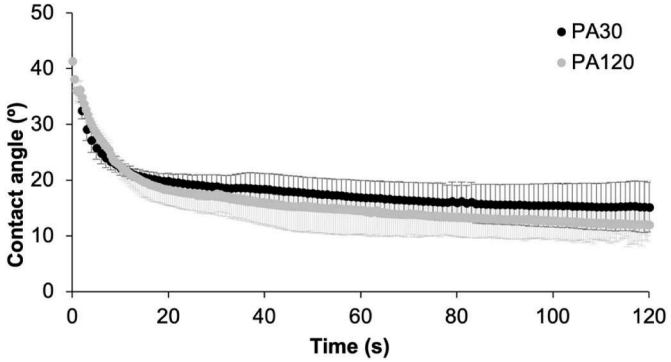

Fig. 8. Dynamic water contact angle profiles obtained for the different adhesive formulations – PA30 and PA120.

Table 2
Initial and final results of the dynamic water contact angles registered for PA30 and PA120.

	PA30	PA120
CA $_{initial}$ (°)	32.49 ± 0.34	41.33 ± 0.50
CA $_{final}$ (°)	15.60 ± 1.99	12.02 ± 2.62

environment at the wound site, enhancing the healing process and improving wound aesthetics, particularly when compared to traditional dry therapies such as gauze, cotton pads, or bandages [44]. The hydrophilic behavior of both materials can be attributed to the incorporation of high-polarity, naturally hydrophilic PEG into the PA composition, which promotes cell adhesion, spreading, and growth on the surface of the wound dressings [45,46].

Surface energy is a key factor influencing the adhesion properties of polymers, as well as their wettability and interaction with biological tissues [47]. It determines the material's ability to spread on or adhere to a surface, which is critical for tissue adhesives. For successful adhesion, a basic thermodynamic criterion must be satisfied: the surface energy of the adhesive must be equal to or lower than that of the substrate (e.g., skin or blood) to ensure favorable wetting and interfacial bonding [48].

To evaluate this, surface energy values of the developed materials were determined using contact angle measurements with liquids of known surface tension. The calculated surface energies, including their polar and dispersive components, are presented in Table 3, along with literature values for skin and blood for comparison.

The obtained results show that the surface energy values are similar for both materials, which are lower than those reported for blood and comparable to those reported for skin. This is a promising indicator of their viability as adhesives, especially on bleeding or moist tissue surfaces, where a lower surface energy facilitates spreading and strong interfacial interaction with the substrate [49]. Moreover, the polar components of the surface energy were higher than the dispersive components, indicating that polar (adhesive) interactions dominate over nonpolar (cohesive) interactions. This favors strong interfacial bonding with polar biological tissues.

Overall, these results support the potential of the synthesized materials to achieve effective adhesion under physiological conditions, particularly in wound sites where the presence of blood or tissue fluids could otherwise compromise bonding.

3.9. Characterization of the cytocompatibility

Besides their physicochemical properties, the photocrosslinked materials' biological compatibility also plays a crucial role in their performance. Therefore, the cytocompatibility of the PA30 and PA120 towards fibroblasts (NHDF) was studied for different incubation time points.

The obtained data showed that PA30 and PA120 had different effects on the NHDF (Fig. 9). When the cells were incubated with the PA30 materials for 1, 3, or 7 days, they displayed a high viability (>79 %). The optical microscopy images also highlighted that the PA30 did not induce changes in the cells' density and morphology (when compared to the control) - Fig. 10. Taken together, this data confirms the good cytocompatibility of the PA30 materials. In stark contrast, the PA120 affected the cells' viability, density, and morphology (Figs. 9 and 10). The distinct behavior of PA30 and PA120 materials towards the NHDF may be related to the different photocrosslinking times (30 s vs. 120 s). Based on the previous data, PA30 materials showed a lower gel content and slightly higher weight loss when incubated in a physiological mimicking medium (Table 1 and Fig. 7). Such distinctive properties are likely to have contributed to the enhanced cytocompatibility of PA30. In line with these observations, in another work [51], unsaturated polyester films with shorter photocrosslinking times also displayed a lower gel content and faster degradability, leading to improved biological compatibility.

Table 3
Surface energies (γ_S) and corresponding dispersive (γ_S^D) and polar (γ_S^P) components of skin, blood, and the prepared materials PA30 and PA120.

Substrate	Surface energies and surface tensions (mN/m)		
	γ_S	γ_S^D	γ_S^P
Skin [49]	38–56	–	–
Blood [50]	68.3	–	–
PA30	53.01 ± 1.84	24.63 ± 3.24	35.01 ± 1.34
PA120	48.88 ± 2.05	28.01 ± 1.95	30.45 ± 2.35

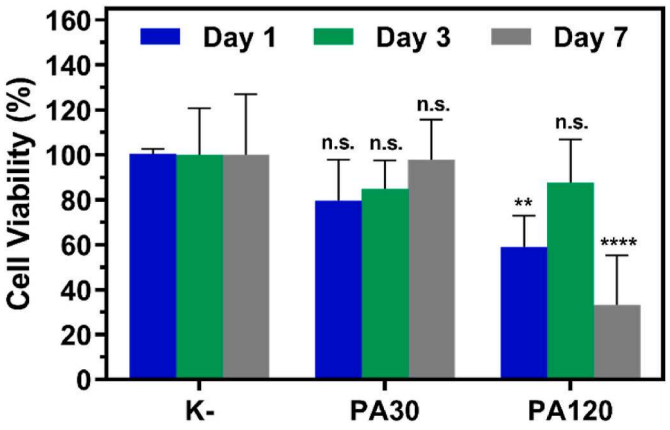

Fig. 9. Viability of NHDF exposed to the PA30 and PA120 materials for 1, 3, and 7 days. K^- represents the negative control. Data are presented as mean ± standard deviation (n = 5). $^{**}p < 0.01$ significant *vs.* the K- of the same incubation time; $^{****}p < 0.0001$ significant *vs.* the K- of the same incubation time; n.s. denotes non-significant vs. the K- of the same incubation time.

4. Conclusions

This study reports the successful synthesis of a novel, solvent-free, UV-crosslinkable tissue adhesive based on PEG functionalized with 2-isocyanatoethyl acrylate (AOI), a monomer with dual reactivity that remains underexplored in biomedical adhesive research. PEG modification was confirmed using ATR-FTIR and ^{1}H NMR spectroscopy. This process yielded low-viscosity polymers, which were subsequently crosslinked under UV irradiation, using the biocompatible photoinitiator Ir2959, forming adhesive films (PA) after only 30 or 120 s of exposure. These films exhibited favorable properties for biomedical use, including high gel content, flexibility, and thermal stability, with low glass transition temperatures, confirming mechanical performance below and at physiological temperatures.

UV exposure time had a minimal impact on the materials' physicochemical behavior, indicating that an efficient crosslinking can be achieved with just 30 s of irradiation, which is a clinically advantageous feature. Dynamic contact angle measurements indicated hydrophilic properties, promoting interaction with biological compounds and aiding wound moisture retention. Surface energy analysis revealed values lower than those reported for blood and comparable to those reported for skin, suggesting strong adhesion to the epidermis or bleeding tissues. Importantly, biological evaluation revealed that PA30 exhibited superior cytocompatibility compared to PA120, maintaining healthier cell behavior and morphology. This difference is likely related to variations in UV exposure time, which influenced crosslinking density and material degradability.

While both formulations showed promising physicochemical performance, PA30 stood out as the most appealing candidate, presenting effective crosslinking, ease of handling, and suitable cytocompatibility.

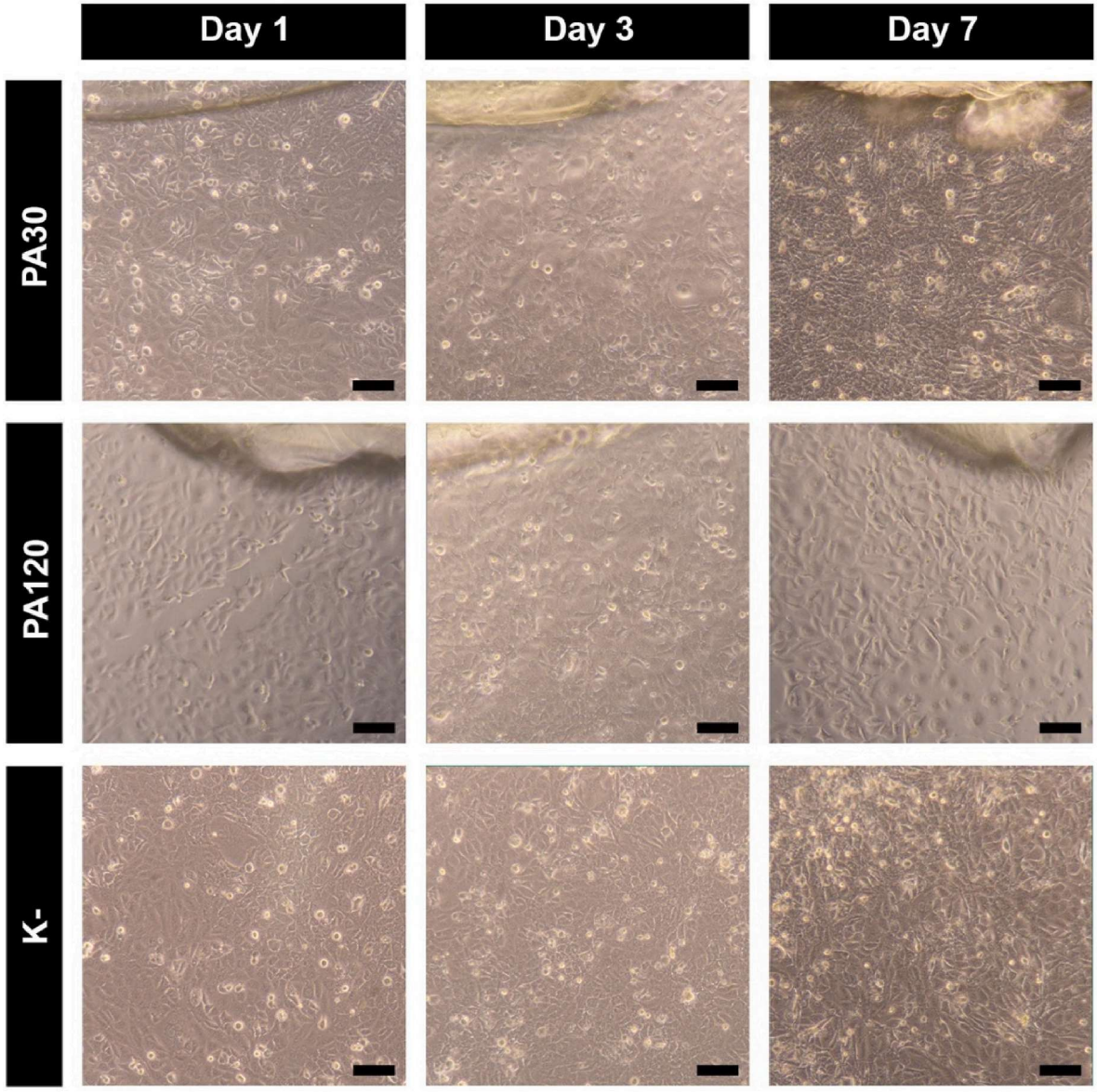

Fig. 10. Optical microscopy images of NHDF incubated with the PA30 and PA120 materials for 1, 3, and 7 days. K^- represents the negative control. The scale bar represents 100 μm.

These findings demonstrate the viability of this PEG–AOI (PA) system as a photocrosslinkable adhesive. Future work will focus on *in vivo* evaluation to assess the performance in relevant biological environments, as well as long-term degradation behavior and wound-healing efficacy. These steps are essential to support clinical translation and to further establish the potential of PA30 for biomedical applications.

CRediT authorship contribution statement

T. Cernadas: Writing – original draft, Methodology, Investigation, Data curation. **M. Ferreira:** Investigation. **B.L. Melo:** Writing – review & editing, Methodology, Investigation, Formal analysis. **D. de Melo-Diogo:** Writing – review & editing, Validation, Methodology, Investigation, Data curation. **I.J. Correia:** Writing – review & editing, Supervision, Resources, Funding acquisition. **P. Ferreira:** Writing – review & editing, Writing – original draft, Visualization, Validation, Supervision, Resources, Project administration, Methodology, Investigation, Funding acquisition, Formal analysis, Data curation, Conceptualization. **P. Alves:** Writing – review & editing, Writing – original draft, Visualization, Validation, Supervision, Resources, Project administration, Methodology, Investigation, Funding acquisition, Formal analysis, Data curation, Conceptualization.

Declaration of competing interest

The authors declare the following financial interests/personal relationships which may be considered as potential competing interests: Patricia Alves reports financial support was provided by Foundation for Science and Technology. Patricia Alves reports a relationship with University of Coimbra that includes: employment. The authors acknowledge FCT (Fundação para a Ciência e Tecnologia, Portugal) for the financial support to CERES (DOI: 10.54499/UIDB/00102/2020 and DOI: 10.54499/UIDP/00102/2020); CERNAS (DOI: 10.54499/UIDP/00681/2020); CICS-UBI (DOI: 10.54499/UIDB/00709/2020 and 10.54499/UIDP/00709/2020); CEMMPRE (DOI: 10.54499/UIDB/00285/2020 and 10.54499/UIDP/00285/2020), AEROG-LAETA (DOI: 10.54499/LA/P/0079/2020 and 10.54499/UIDB/50022/2020) and ARISE (DOI: 10.54499/LA/P/0112/2020). FCT is also acknowledged

for the PhD grant 2022.09787.BD (to T. Cernadas) and 2021.06044.BD (to Bruna L. Melo), for the Junior Researcher contract 2021.00590.CEECIND (DOI: 10.54499/2021.00590.CEECIND/CP1661/CT0001; to Duarte de Melo-Diogo), and for the institutional scientific employment program-contract CEECINST/00077/2021 (to P. Ferreira) and CEECINSTLA/00023/2022 (to P. Alves). The FCT funded Wastesilk (PTDC/BTABTA/0696/2020), GRAPHY (2022.06320.PTDC; DOI: 10.54499/2022.06320.PTDC) and SmartLipoGel (2022.02495.PTDC; DOI: 10.54499/2022.02495.PTDC) projects are also acknowledged. 1H NMR data were obtained at the Nuclear Magnetic Resonance Laboratory of the Coimbra Chemistry Centre (www.nmrccc.uc.pt) from University of Coimbra, Portugal, supported in part by grant REEQ/481/QUI/2006 from FCT, POCI-2010, and FEDER, Portugal. If there are other authors, they declare that they have no known competing financial interests or personal relationships that could have appeared to influence the work reported in this paper.

Acknowledgements

The authors acknowledge FCT (Fundação para a Ciência e Tecnologia, Portugal) for the financial support to CERES (DOI: 10.54499/UIDB/00102/2020 and DOI: 10.54499/UIDP/00102/2020); CERNAS (DOI: 10.54499/UIDP/00681/2020); CICS-UBI (DOI: 10.54499/UIDB/00709/2020 and 10.54499/UIDP/00709/2020); CEMMPRE (DOI: 10.54499/UIDB/00285/2020 and 10.54499/UIDP/00285/2020), AEROG-LAETA (DOI: 10.54499/LA/P/0079/2020 and 10.54499/UIDB/50022/2020) and ARISE (DOI: 10.54499/LA/P/0112/2020). FCT is also acknowledged for the PhD grant 2022.09787.BD (to T. Cernadas) and 2021.06044.BD (DOI: 10.54499/2021.06044.BD; to Bruna L. Melo), for the Junior Researcher contract 2021.00590.CEECIND (DOI: 10.54499/2021.00590.CEECIND/CP1661/CT0001; to Duarte de Melo-Diogo), and for the institutional scientific employment program-contract CEECINST/00077/2021 (to P. Ferreira) and CEECINSTLA/00023/2022 (to P. Alves). The FCT funded Wastesilk (PTDC/BTABTA/0696/2020), GRAPHY (2022.06320.PTDC; DOI: 10.54499/2022.06320.PTDC) and SmartLipoGel (2022.02495.PTDC; DOI: 10.54499/2022.02495.PTDC) projects are also acknowledged. For the purpose of Open Access, the authors have applied a CC-BY public copyright license to any Author's Accepted Manuscript (AAM) version arising from this submission. ^{1}H NMR data were obtained at the Nuclear Magnetic Resonance Laboratory of the Coimbra Chemistry Centre (www.nmrccc.uc.pt), Universidade de Coimbra, supported in part by grant REEQ/481/QUI/2006 from FCT, POCI-2010, and FEDER, Portugal.

Data availability

Data will be made available on request.

References

[1] S. Ebnesajjad, A.H. Landrock, Chapter 10 - adhesives for medical and dental applications, in: S. Ebnesajjad, A.H. Landrock (Eds.), Adhes. Technol. Handb, third ed., William Andrew Publishing, 2015, pp. 258–296, https://doi.org/10.1016/b978-0-323-35595-7.00010-3.

[2] K. Modaresifar, S. Azizian, A. Hadjizadeh, Nano/biomimetic tissue adhesives development: from research to clinical application, Polym. Rev. 56 (2016) 329–361, https://doi.org/10.1080/15583724.2015.1114493.

[3] D.R.S. Travassos, J.M.C. Santos, C.M.S.G. Baptista, D.S. Marques, P. Ferreira, M. H. Gil, et al., Engineering star-shaped lactic acid oligomers to develop novel functional adhesives, J. Mater. Res. 33 (2018) 1463–1474, https://doi.org/10.1557/jmr.2018.73.

[4] M. Kharaziha, T. Scheibel, S. Salehi, Multifunctional naturally derived bioadhesives: from strategic molecular design toward advanced biomedical applications, Prog. Polym. Sci. 150 (2024) 101792, https://doi.org/10.1016/j.progpolymsci.2024.101792.

[5] G.Y. Han, H.W. Kwack, Y.H. Kim, Y.H. Je, H.J. Kim, C.S. Cho, Progress of polysaccharide-based tissue adhesives, Carbohydr. Polym. 327 (2024), https://doi.org/10.1016/j.carbpol.2023.121634.

[6] Q. Su, D. Wei, W. Dai, Y. Zhang, Z. Xia, Designing a Castor oil-based polyurethane as bioadhesive, Colloids Surf. B Biointerfaces 181 (2019) 740–748, https://doi.org/10.1016/j.colsurfb.2019.06.032.

[7] A. Chandrasekharan, K.Y. Seong, S.G. Yim, S. Kim, S. Seo, J. Yoon, et al., In situ photocrosslinkable hyaluronic acid-based surgical glue with tunable mechanical properties and high adhesive strength, J. Polym. Sci. Part A Polym Chem 57 (2019) 522–530, https://doi.org/10.1002/pola.29290.

[8] A. Bal-Ozturk, B. Cecen, M. Avci-Adali, S.N. Topkaya, E. Alarcin, G. Yasayan, et al., Tissue adhesives: from research to clinical translation, Nano Today 36 (2021), https://doi.org/10.1016/j.nantod.2020.101049.

[9] X. Yang, X. Li, Z. Wu, L. Cao, Photocrosslinked methacrylated natural macromolecular hydrogels for tissue engineering: a review, Int. J. Biol. Macromol. 246 (2023), https://doi.org/10.1016/j.ijbiomac.2023.125570.

[10] M. Santos, T. Cernadas, P. Martins, S.P. Miguel, I.J. Correia, P. Alves, et al., Polyester-based photocrosslinkable bioadhesives for wound closure and tissue regeneration support, React. Funct. Polym. 158 (2021) 104798, https://doi.org/10.1016/j.reactfunctpolym.2020.104798.

[11] P. Ferreira, J, J.F.F.J. Coelho, M. H, Photocrosslinkable polymers for biomedical applications, Biomed. Eng. - Front. Challenges (2011), https://doi.org/10.5772/18752. InTech.

[12] A. Zennifer, S. Manivannan, S. Sethuraman, S.G. Kumbar, D. Sundaramurthi, 3D bioprinting and photocrosslinking: emerging strategies & future perspectives, Biomater. Adv. 134 (2022) 112576, https://doi.org/10.1016/j.msec.2021.112576.

[13] T. Cernadas, M. Santos, S. Miguel, I. Correia, P. Alves, P. Ferreira, Photocurable polymeric blends for surgical application, Materials 13 (2020) 5681, https://doi.org/10.3390/ma13245681.

[14] T.M. Cernadas, F.A.M.M. Gonçalves, P. Alves, S.P. Miguel, C. Cabral, I.J. Correia, et al., Preparation of biodegradable functionalized polyesters aimed to be used as surgical adhesives, Eur. Polym. J. 117 (2019), https://doi.org/10.1016/j.eurpolymj.2019.05.019.

[15] A.T. Metters, K.S. Anseth, C.N. Bowman, Fundamental studies of a novel, biodegradable PEG-b-PLA hydrogel, Polymer (Guildf.) 41 (2000) 3993–4004, https://doi.org/10.1016/S0032-3861(99)00629-1.

[16] J. Yang, H. Yu, L. Wang, J. Liu, X. Liu, Y. Hong, et al., Advances in adhesive hydrogels for tissue engineering, Eur. Polym. J. 172 (2022) 111241, https://doi.org/10.1016/j.eurpolymj.2022.111241.

[17] H. Zhang, T. Zhao, P. Duffy, Y. Dong, A.N. Annaidh, E.O. Cearbhaill, et al., Hydrolytically degradable hyperbranched PEG-polyester adhesive with low swelling and robust mechanical properties, Adv. Healthcare Mater. 4 (2015) 2260–2268, https://doi.org/10.1002/adhm.201500406.

[18] F. Scognamiglio, A. Travan, I. Rustighi, P. Tarchi, S. Palmisano, E. Marsich, et al., Adhesive and sealant interfaces for general surgery applications, J. Biomed. Mater. Res. Part B Appl Biomater 104 (2016) 626–639, https://doi.org/10.1002/jbm.b.33409.

[19] P. Ferreira, J.F.J. Coelho, M.H. Gil, Development of a new photocrosslinkable biodegradable bioadhesive, Int. J. Pharm. 352 (2008) 172–181, https://doi.org/10.1016/j.ijpharm.2007.10.026.

[20] J.R. Choi, K.W. Yong, J.Y. Choi, A.C. Cowie, Recent advances in photo-crosslinkable hydrogels for biomedical applications, Biotechniques 66 (2019) 40–53, https://doi.org/10.2144/btn-2018-0083.

[21] R.N. Ghosh, J.B.R. Thomas, N.G.D. V, A. Janardanan, P.K. Namboothiri, et al., An insight into synthesis, properties and applications of gelatin methacryloyl hydrogel for 3D bioprinting, Mater. Adv. 4 (2023) 5496–5529, https://doi.org/10.1039/D3MA00715D.

[22] A.D.R. Pontinha, B.B. Moreira, B.L. Melo, D de Melo-diogo, I.J. Correia, P. Alves, Silica aerogel-polycaprolactone scaffolds for bone tissue engineering, Int. J. Mol. Sci. 24 (2023) 1–18, https://doi.org/10.3390/ijms241210128.

[23] M.N. Dinh, M. Hitomi, Z.A. Al-Turaihi, J.G. Scott, Alamar blue assay optimization to minimize drug interference and inter assay viability, MethodsX 13 (2024) 103024, https://doi.org/10.1016/j.mex.2024.103024.

[24] J. Bernardini, D. Licursi, I. Anguillesi, P. Cinelli, M.-B. Coltelli, C. Antonetti, et al., Exploitation of Arundo donax L. hydrolysis residue for the green synthesis of flexible polyurethane foams, Bioresources 12 (2017), https://doi.org/10.15376/biores.12.2.3630-3655.

[25] D.S. Marques, J.M.C. Santos, P. Ferreira, T.R. Correia, I.J. Correia, M.H. Gil, et al., Photocurable bioadhesive based on lactic acid, Mater. Sci. Eng., C 58 (2016) 601–609, https://doi.org/10.1016/j.msec.2015.09.009.

[26] T. Cernadas, M. Santos, F.A.M.M. Gonçalves, P. Alves, T.R. Correia, I.J. Correia, et al., Functionalized polyester-based materials as UV curable adhesives, Eur. Polym. J. 120 (2019) 109196, https://doi.org/10.1016/j.eurpolymj.2019.08.023.

[27] J.L. Pasek-allen, R.K. Wilharm, J.C. Bischof, V.C. Pierre, NMR characterization of polyethylene glycol conjugates for nanoparticle functionalization, ACS Omega 8 (2023) 4331–4336, https://doi.org/10.1021/acsomega.2c07669.

[28] P. Duval, B. Flan, T. Burnouf, J.J. Huart, [Validation of rheological properties of fibrin glue: Biocol-Human Thrombin], Ann. Pharm. Fr. 52 (1994) 43–52.

[29] T. Nagata, Y. Harada, M. Arai, T. Hirose, H. Kondo, Polyethylene glycol-based synthetic hydrogel sealant for filtration bleb leaks: an in vivo and histologic study, Transl. Vis. Sci. Technol. 9 (2020) 24, https://doi.org/10.1167/tvst.9.6.24.

[30] W. Li, M. Lin, C. Wang, Y. Lu, Y. Sui, X. Ni, et al., In vitro enzymatic degradation of the PTMC/cross-linked PEGDA blends, Front. Bioeng. Biotechnol. 11 (2023), https://doi.org/10.3389/fbioe.2023.1253221.

[31] G. Burke, Z. Cao, D.M. Devine, I. Major, Preparation of biodegradable polyethylene glycol dimethacrylate hydrogels via thiol-ene chemistry, Polymers 11 (2019) 1339, https://doi.org/10.3390/polym11081339.

[32] A.P. Duarte, J.F. Coelho, J.C. Bordado, M.T. Cidade, M.H. Gil, Surgical adhesives: systematic review of the main types and development forecast, Prog. Polym. Sci. 37 (2012) 1031–1050, https://doi.org/10.1016/j.progpolymsci.2011.12.003.

[33] S.P. Miguel, D. Simões, A.F. Moreira, R.S. Sequeira, I.J. Correia, Production and characterization of electrospun silk fibroin based asymmetric membranes for

wound dressing applications, Int. J. Biol. Macromol. 121 (2019) 524–535, https://doi.org/10.1016/j.ijbiomac.2018.10.041.
[34] P.J.M.M. Bouten, M. Zonjee, J. Bender, S.T.K.K. Yauw, H. Van Goor, J.C.M.M. Van Hest, et al., The chemistry of tissue adhesive materials, Prog. Polym. Sci. 39 (2014) 1375–1405, https://doi.org/10.1016/j.progpolymsci.2014.02.001.
[35] N.A. Peppas, P. Bures, W. Leobandung, H. Ichikawa, Hydrogels in pharmaceutical formulations, Eur. J. Pharm. Biopharm. 50 (2000) 27–46, https://doi.org/10.1016/S0939-6411(00)00090-4.
[36] Q.T. Nguyen, Y. Hwang, A.C. Chen, S. Varghese, R.L. Sah, Cartilage-like mechanical properties of poly (ethylene glycol)-diacrylate hydrogels, Biomaterials 33 (2012) 6682–6690, https://doi.org/10.1016/j.biomaterials.2012.06.005.
[37] T. Vuocolo, R. Haddad, G.A. Edwards, R.E. Lyons, N.E. Liyou, J.A. Werkmeister, et al., A highly elastic and adhesive gelatin tissue sealant for gastrointestinal surgery and Colon anastomosis, J. Gastrointest. Surg. 16 (2012) 744–752, https://doi.org/10.1007/s11605-011-1771-8.
[38] W.D. Spotnitz, S. Burks, Hemostats, sealants, and adhesives: components of the surgical toolbox, Transfusion 48 (2008) 1502–1516, https://doi.org/10.1111/j.1537-2995.2008.01703.x.
[39] Z. Li, D. Zhou, Acrylate-based PEG hydrogels with ultrafast biodegradability for 3D cell culture, Biomacromolecules 25 (2024) 6195–6202, https://doi.org/10.1021/acs.biomac.4c01051.
[40] G.Y. Han, S.K. Hwang, K.H. Cho, H.J. Kim, C.S. Cho, Progress of tissue adhesives based on proteins and synthetic polymers, Biomater. Res. 27 (2023) 1–21, https://doi.org/10.1186/s40824-023-00397-4.
[41] P.J. Martens, S.J. Bryant, K.S. Anseth, Tailoring the degradation of hydrogels formed from multivinyl poly(ethlene glycol) and poly(vinyl alcohol) macromers for cartilage tissue engineering, Biomacromolecules 4 (2003) 283–292, https://doi.org/10.1021/bm025666v.
[42] X. Ma, S. Oyamada, T. Wu, M.P. Robich, H. Wu, X. Wang, et al., In vitro and in vivo degradation of poly(D, L-lactide-co-glycolide)/amorphous calcium phosphate copolymer coated on metal stents, J. Biomed. Mater. Res., Part A 96A (2011) 632–638, https://doi.org/10.1002/jbm.a.33016.
[43] M. Stamm, Characterization techniques, in: M. Stamm (Ed.), Polym. Surfaces Interfaces, 2008, pp. 1–16, https://doi.org/10.1007/978-3-540-73865-7. Berlin, Heidelberg: Springer Berlin Heidelberg.
[44] J.P.E. Junker, R.A. Kamel, E.J. Caterson, E. Eriksson, Clinical impact upon wound healing and inflammation in moist, wet, and dry environments, Adv. Wound Care 2 (2013) 348–356, https://doi.org/10.1089/wound.2012.0412.
[45] S.P. Miguel, M.P. Ribeiro, H. Brancal, P. Coutinho, I.J. Correia, Thermoresponsive chitosan-agarose hydrogel for skin regeneration, Carbohydr. Polym. 111 (2014) 366–373, https://doi.org/10.1016/j.carbpol.2014.04.093.
[46] A.A. D'souza, R. Shegokar, Polyethylene glycol (PEG): a versatile polymer for pharmaceutical applications, Expet Opin. Drug Deliv. 13 (2016) 1257–1275, https://doi.org/10.1080/17425247.2016.1182485.
[47] P. Alves, R. Cardoso, T.R. Correia, B.P. Antunes, I.J. Correia, P. Ferreira, Surface modification of polyurethane films by plasma and ultraviolet light to improve haemocompatibility for artificial heart valves, Colloids Surf. B Biointerfaces 113 (2014), https://doi.org/10.1016/j.colsurfb.2013.08.039.
[48] S. Banerjee, P. Chattopadhyay, A. Ghosh, P. Datta, V. Veer, Aspect of adhesives in transdermal drug delivery systems, Int. J. Adhesion Adhes. 50 (2014) 70–84, https://doi.org/10.1016/j.ijadhadh.2014.01.001.
[49] S. Venkatraman, R. Gale, Skin adhesives and skin adhesion. 1. Transdermal drug delivery systems, Biomaterials 19 (1998) 1119–1136, https://doi.org/10.1016/S0142-9612(98)00020-9.
[50] A. Kratochvíl, E. Hrnčíř, Correlation between the blood surface tension and the activity of some enzymes, Physiol. Res. 50 (2001) 433–437, https://doi.org/10.33549/physiolres.930058.
[51] T. Cernadas, J. Pereira, B.L. Melo, D. de Melo-Diogo, I.J. Correia, P. Alves, et al., Renewable photo-cross-linkable polyester-based biomaterials: synthesis, characterization, and cytocompatibility assessment, Biomacromolecules 25 (2024) 7134–7145, https://doi.org/10.1021/acs.biomac.4c00599.